1 # Geometrical determinant of nonlinear synaptic integration in
2 # human cortical pyramidal neurons
3

4 Jaeyoung Yoon[1,2,*], et al.[†]

5 [1] McGovern Institute for Brain Research, Massachusetts Institute of Technology, Cambridge, MA 02139, USA.
6 [2] Present address: F. M. Kirby Neurobiology Center, Boston Children's Hospital, & Harvard Medical School,
7 Boston, MA 02115, USA.
8 [*] Correspondence: jy.yoon@tch.harvard.edu
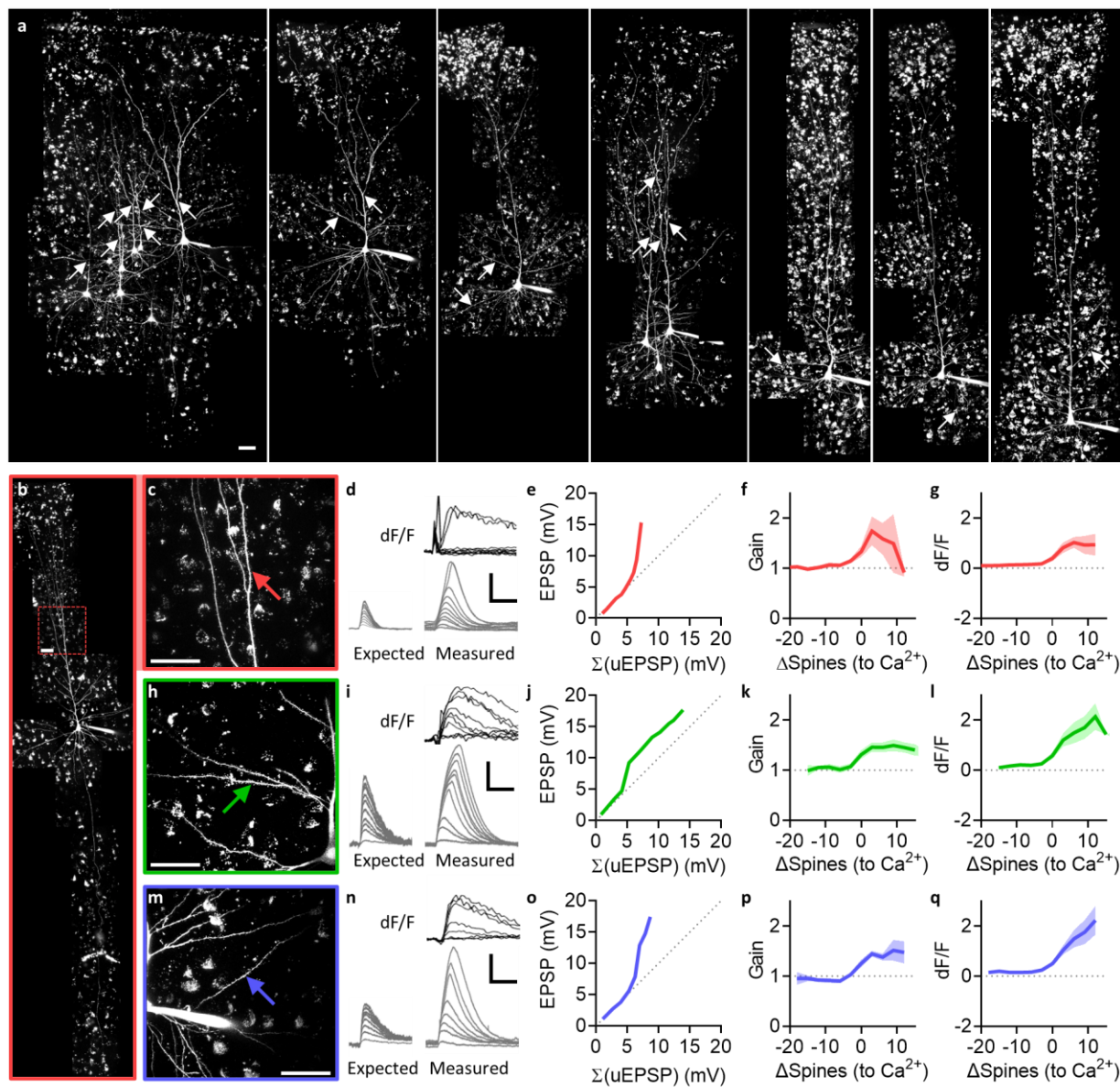9 [†] *Full author list to be determined*

10

Fig. 1

Figure 1. Synaptic integration at human neocortical layer 2/3 pyramidal neurons (L2/3 PN). **(a)** Representative examples of L2/3 PNs. Scale bar, 50 μm. Arrows indicate the center of synaptic spine clusters that were activated by 2-photon glutamate uncaging (2PGU), which typically spanned approximately 30-40 μm along the length of the branch. The high background is caused by lipofuscin aggregates on the somata of human neurons; see **Fig. 4** for comparison. **(b-c)** Representative example of an L2/3 PN, with 2PGU at the apical tuft. **(d)** Representative examples of expected EPSP (left), calculated from the arithmetic sum of unitary EPSP (uEPSP) recorded from each spine, and measured EPSP (right, bottom) recorded by quasi-simultaneous activation of spines shown in panel **c**, along with the associated fractional change in Ca^{2+} fluorescence (dF/F) obtained by intracellular calcium imaging at the parent dendrite (right, top). Scale bars, 50 ms, 5 mV, 1.0 dF/F. **(e)** Representative example of measured EPSP, plotted against the arithmetic sum of uEPSPs, from the activation of the same spines as shown in panels **b-d**. **(f)** Grouped average of synaptic gain from all apical tuft dendrites (n = 24). Gain was defined by the ratio of measured vs. expected EPSP. The number of activated spines were aligned to the threshold at which Ca^{2+} signal was first observed. **(g)** Grouped average of dF/F, associated with data shown in panel **f**. **(h-l)** Similar to panels **c-g**, but from oblique dendrites (n = 16) branching from the apical trunk. **(m-q)** Similar to panels **c-g** or **h-l**, but from basal dendrites (n = 20) branching from the soma.

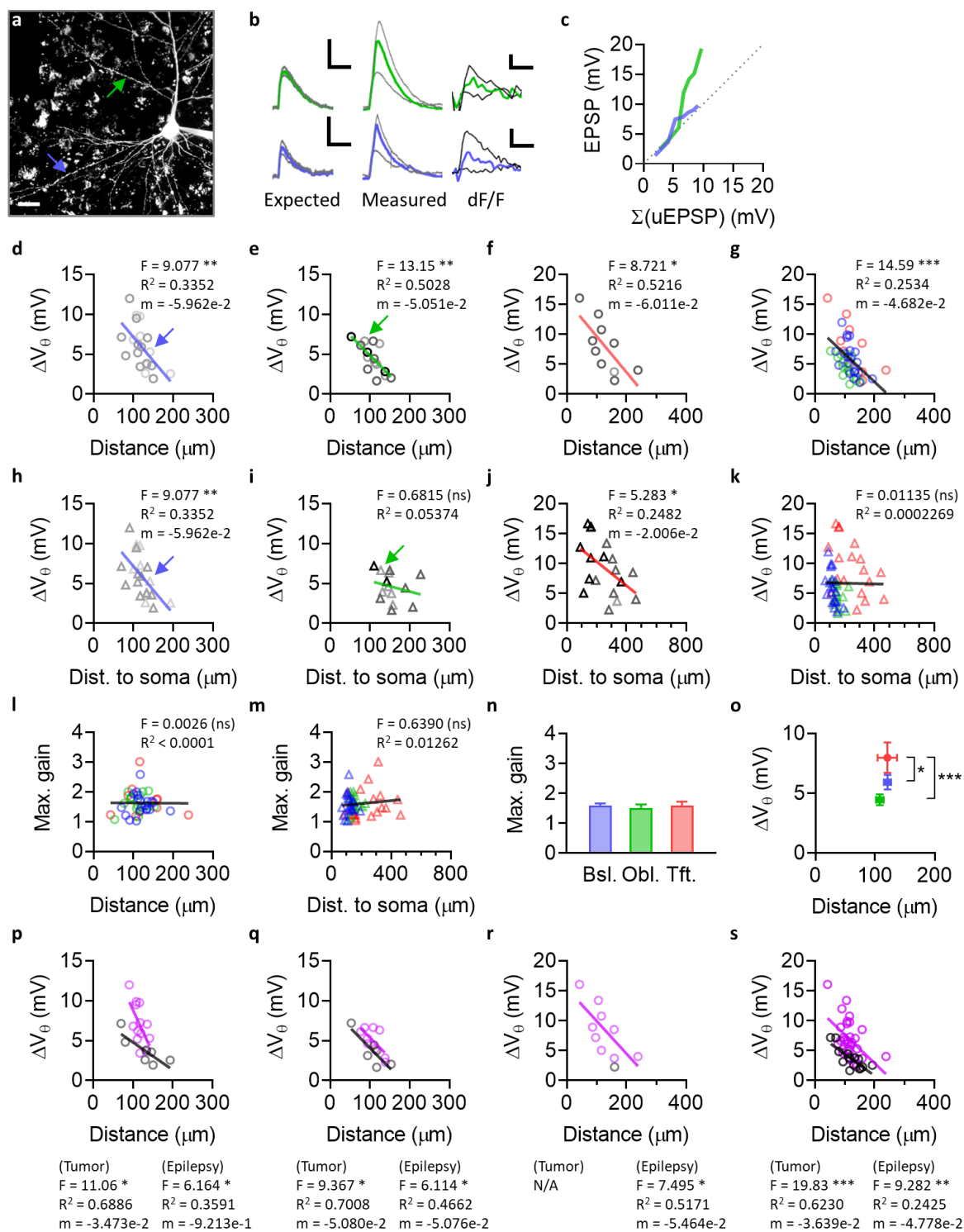**Fig. 2**

Figure 2. Somatic depolarization at nonlinearity threshold (ΔV_θ) is determined by the distance between the synapse and the nearest point on the apical trunk or the soma. **(a)** Representative example of a human L2/3 PN. Two different uncaging locations, one on a basal dendrite (blue) and another on an oblique dendrite (green), are indicated by arrows. Scale bar, 50 µm. **(b)** Representative traces of expected and measured EPSP, along with associated dF/F, from the branches shown in panel **a**. Scale bars, 50 ms, 5 mV, 0.5 (bottom) or 0.1 (top) dF/F. **(c)** Measured EPSP vs. expected EPSP from the sum of uEPSPs, from the same branches shown in panels **a-b**. **(d-g)** Somatic depolarization at nonlinearity threshold (ΔV_θ), plotted against synaptic distance. ΔV_θ was defined as the expected somatic EPSP at local nonlinearity threshold indicated by the local Ca^{2+} signal; the expected EPSP from the sum of uEPSPs was used instead of the measured EPSP to determine the correct threshold irrespective of the nonlinear gain. Synaptic distance was defined as the curvilinear projected distance along the dendrite from the synapse to the nearest point on the apical trunk or the soma. Notably, the linear regressions in panels **d-g** had similar slopes in all groups (F = 0.06380, P = 0.9383). **(d)** ΔV_θ at basal dendrites vs. distance (to soma). Shades of symbols indicate branch order (1st to 4th, darker to lighter, throughout panels **d-f**), which was not correlated with ΔV_θ. **(e)** ΔV_θ at oblique dendrites vs. distance (to the branch point at the apical trunk). **(f)** ΔV_θ at apical tuft dendrites vs. distance to (to the branch point at the apical trunk, i.e. nexus). **(g)** Data shown in panels **d-f**, overlaid for comparison. **(h-k)** similar to panels **d-g**, but plotted instead against distance to soma; by definition of synaptic distance used in panels **d-g**, panel **h** is identical to panel **d** (for basal dendrites only). Note that in panel **j**, synapses located at the nexus are also included, whereas they were excluded from panel **f** due to having zero synaptic distance as defined. **(l)** Maximum gain vs. synaptic distance, to the nearest point on the apical trunk or the soma. **(m)** Maximum gain vs. distance to soma. **(n)** Maximum gain at basal, oblique, and tuft dendrites. **(o)** Average ΔV_θ at basal, oblique, and tuft dendrites. **(p-s)** Same data as in panels **d-g**, but grouped separately by tumor (black) or epilepsy (purple). Neurons from the cortex associated with epilepsy had a tendency of higher ΔV_θ for a given synaptic distance, compared to those from tumor tissue.
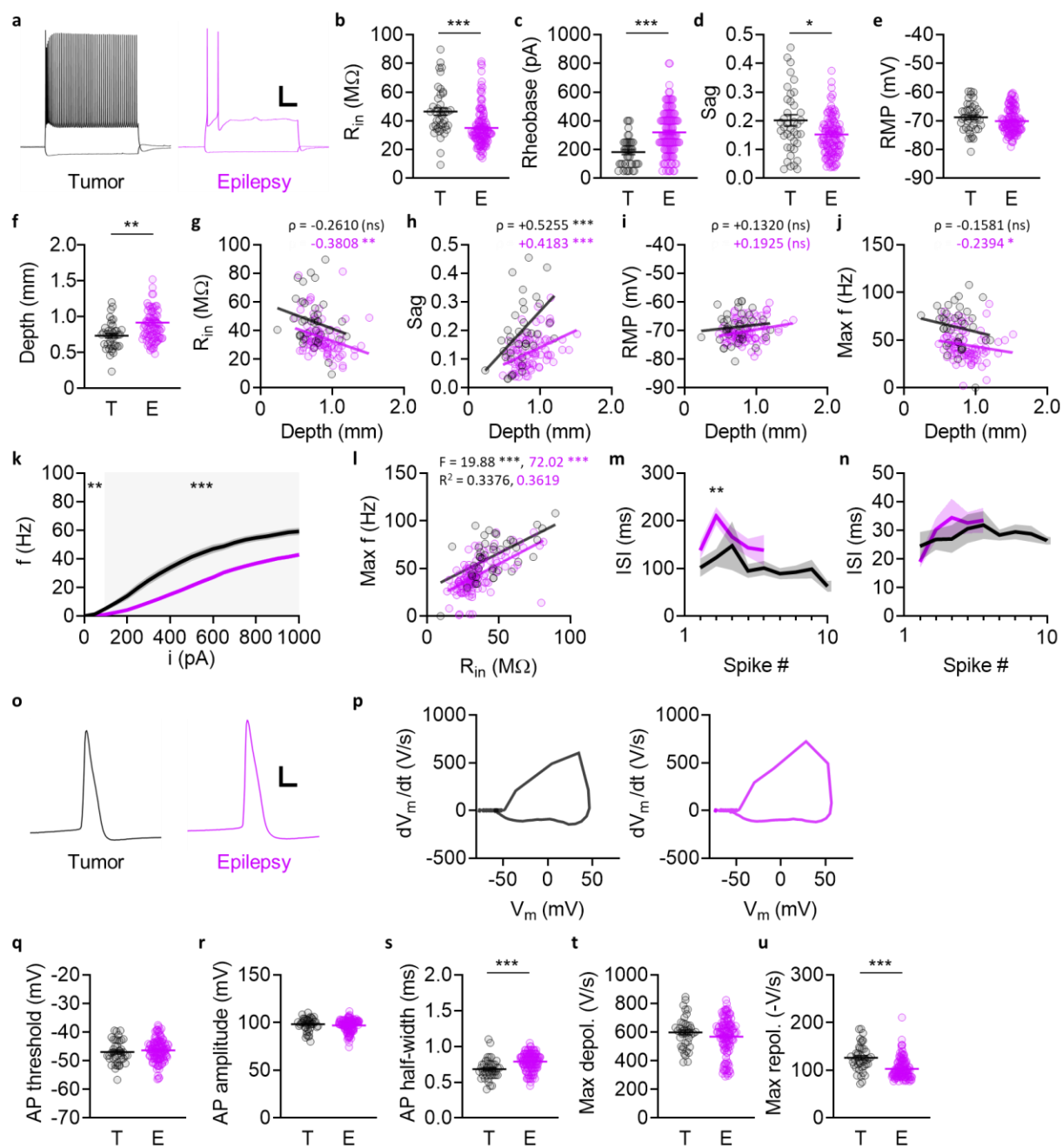
Fig. 3

Figure 3. Intrinsic membrane properties of human L2/3 PN, from tumor (black) or epilepsy (purple). For more detailed patient and tissue information, see **Table 1**. Note that tissue from both tumor and epilepsy patients originated from areas determined to be nonpathological, but removed as part of the surgical procedure. **(a)** Representative traces of membrane potential responses to somatic step current injection (-250 pA, +1000 pA). Scale bar, 20 mV, 200 ms. The example to the right was taken from the same cell as in **Fig. 1a**. **(b)** Input resistance (R_{in}). See methods for R_{in} calculation. **(c)** Rheobase, with current step resolution of 50 pA. **(d)** Sag ratio. See methods for the definition of sag ratio. **(e)** Resting membrane potential (RMP). **(f)** Sampling bias in the cortical depths of recorded L2/3 PNs included in the current study. Cortical depth of a recorded cell was defined as the linear distance between the pial surface and the center of the mass of the somatic boundary, extrapolated from the line connecting the soma and the nexus. For all measurements of distance, the position of the soma was defined as the center of mass of its boundary. The depth of one outlier in the tumor group (235 μm) and its identity as an L2/3 PN was verified with the whole-cell 2-photon image of the cell along with neighboring L2/3 PNs deeper within the cortex, all of which had dendritic arbors that were intact up to the pia mater and in plane. **(g-j)** Intrinsic membrane properties, plotted against cortical depth. **(g)** R_{in}. **(h)** Sag ratio. **(i)** RMP. **(j)** Peak firing rate. **(k)** Firing frequency in response to somatic current injection. L2/3 PN firing frequency was significantly lower in epilepsy compared to tumor ($P < 0.001$ each for all $i \geq 100$ (pA), $P < 0.01$ for $i = 50$ (pA)). **(l)** Peak firing rate, plotted against R_{in}. **(m)** Inter-spike interval (ISI) at rheobase. **(n)** ISI at 2*rheobase. **(o)** Representative traces of single action potentials (AP) from human L2/3 PNs. For each cell, the first action potential generated at rheobase was taken for analysis. Scale bar, 20 mV, 1 ms. The example to the right was taken from the same cell as in **Fig. 2a**. **(p)** Example AP waveforms presented as dV/dt plots, calculated from the same traces as in panel **o**. **(q)** AP threshold. AP threshold was defined as the V_m at which dV/dt crossed 10 (V/s). **(r)** AP amplitude (RMP to AP peak). **(s)** AP half-width. **(t)** Maximum rate of depolarization. **(u)** Maximum rate of repolarization.

Fig. 4
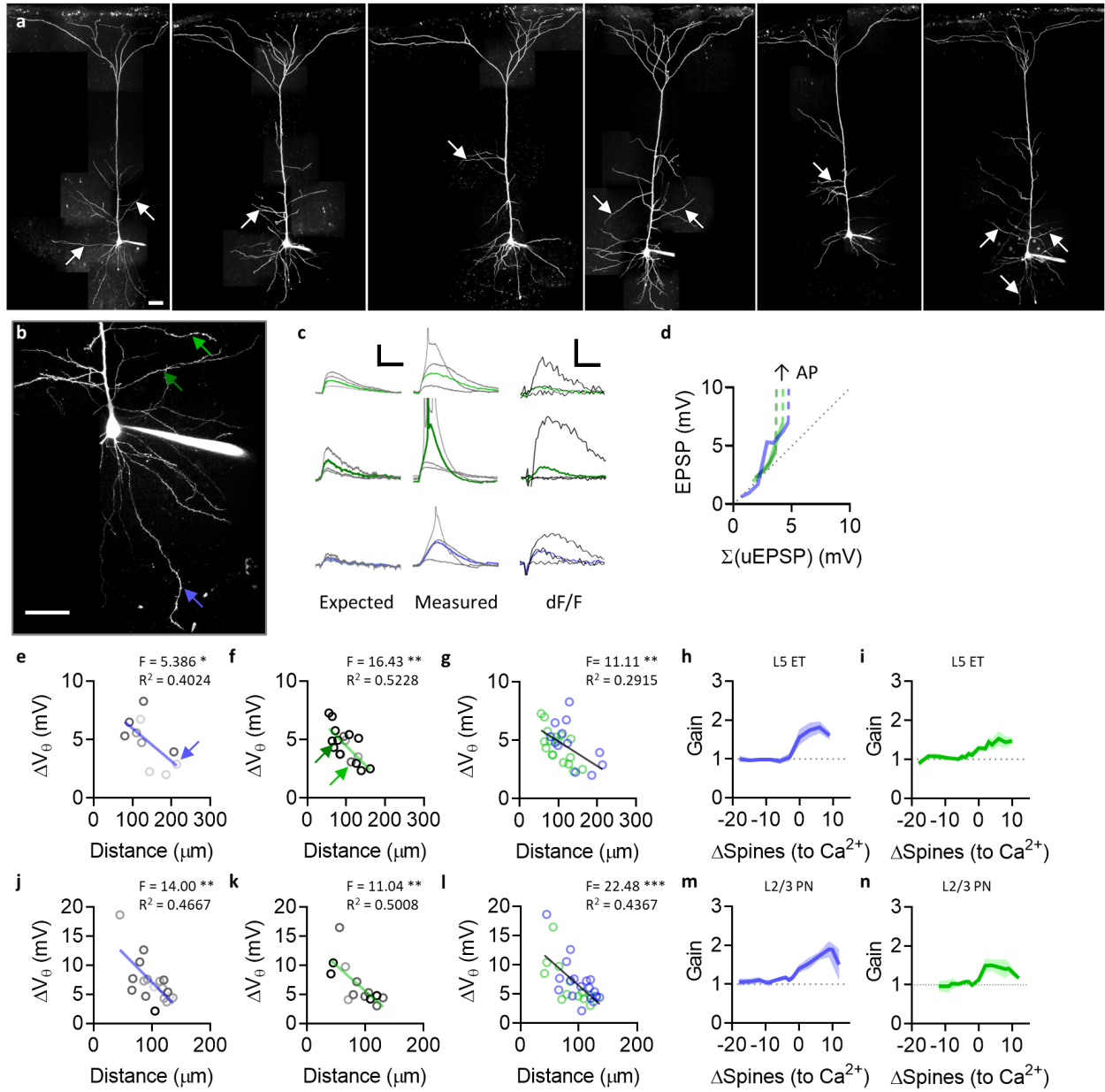
Figure 4. Somatic depolarization at nonlinearity threshold (ΔV_θ) is linearly correlated to synaptic distance from the nearest point on the apical trunk or the soma, in rodents as well as in humans, and for both supragranular and infragranular cortical pyramidal neurons. **(a)** Representative example of a rat L5 ET PN, from the temporal association area (TeA). Three different uncaging locations, one on a basal dendrite and two on separate oblique dendrites, are indicated by arrows. Scale bar, 50 μm. **(b)** Representative traces from the uncaging locations shown in panel a. Scale bars, 50 ms, 5 mV, 0.5 dF/F. **(c)** Measured EPSP vs. expected EPSP from the sum of uEPSPs, from the branches shown in panels **a-b**. **(d-f)** ΔV_θ vs. distance to primary structure, in rat L5 ET. **(d)** Basal dendrites. **(e)** Oblique dendrites. **(f)** Data shown in panels **d-e**, overlaid for comparison. **(g)** Synaptic gain, at basal dendrites shown in panel **d**. **(h)** Synaptic gain, at oblique dendrites shown in panel **e**. **(i-m)** Similar to panels **d-h**, but from rat L2/3 PNs instead of L5 ET. **(i)** Basal dendrites. **(j)** Oblique dendrites. **(k)** Data shown in panels **i-j**, overlaid for comparison. **(l)** Synaptic gain, at basal dendrites shown in panel **i**. **(m)** Synaptic gain, at oblique dendrites shown in panel **j**.

102 **Table 1**

ID	Age	Sex	Area	Hemi.	Medications (AED)	Diagnosis	n (cells/humans)
BA14	-	-	ATL	-	-	Epilepsy	6
BA27	-	-	TL	-	-	Epilepsy	6
BB05	22	M	FL	-	-	Epilepsy	1
BF30	34	F	TL	-	-	Epilepsy	1
BI30	-	-	TL	-	-	Epilepsy	3
BJ04	-	-	TL	-	-	Epilepsy	3
BJ06	-	-	FL	-	-	Epilepsy	1
BK02	55	M	ATL	R	Le	Tumor	10
BK05	32	M	TL	L	Cb, Le, O, T	Epilepsy	2
BK10	71	F	TL	R	-	Tumor	13
BK18	46	M	FL	L	Ce, O, Ph	Epilepsy	7
BL06	71	M	TL	R	-	Epilepsy	13
CC07	33	M	FL	R	B, Lc, Lo	Epilepsy	12
CC17	23	F	ATL	R	Cn, G, Lm, Le, Lo, T, Z	Epilepsy	43*
CC31	24	M	ATL	R	Lc, Le, O, T	Epilepsy	1
CG05	18	F	TL	R	Cb, G, Lm, Le, O, T	Epilepsy	6
CH15	57	F	TL	R	Le	Tumor	9
CH16	24	M	TL	R	E, G, Lm, Le, O, Pe	Epilepsy	16
CI08	30	M	TL	L	Lm, Le	Epilepsy	1
DA31	72	F	TL	R	-	Tumor	4
DB16	31	M	TL	R	-	Epilepsy	7
DC15	71	M	TL	R	-	Tumor	7
						(Tumor)	43/5
						(Epilepsy)	119/17
						(Total)	162/22

Abbreviations:

B, brivaracetam; Ce, cenobamate; Cb, clobazam; Cn, clonazepam; E, eslicarbazepine; G, gabapentin; Lc, lacosamide; Lm, lamotrigine; Le, levetiracetam; Lo, lorazepam; O, oxcarbazepine; Pe, perampanel; Ph, phenytoin; T, topiramate; Z, zonisamide; -, not available (not applicable or unknown). Note that only limited information was made available for a subset of cases (n = 21/7, from a total of 162/22 (cells/humans)).

* Recorded up to 120 h post-resection (typically 24 to 48 h)

103 **Table 1.** Patient and tissue information.

Methods

Brain slice preparation

For human brain slices, tissue resected from patients was immediately placed in an ice-cold solution at the operating theater. The cutting solution used for transport and slicing contained (in mM): 165 sucrose, 20 HEPES, 25 $NaHCO_3$, 2.5 KCl, 1.25 NaH_2PO_4, 20 D-glucose, 5 sodium ascorbate, 3 sodium pyruvate, 0.5 $CaCl_2$, 7 $MgCl_2$, pH adjusted to 7.3 with NaOH, 300-310 mOsm. All materials were obtained from Sigma-Aldrich unless otherwise specified. The tissue bottle was kept in a thermally insulated container filled with ice packs and transported from the operating room at Massachusetts General Hospital (MGH) or Brigham and Women's Hospital (BWH) to the laboratory at Massachusetts Institute of Technology (MIT) within 25 minutes. The tissue block was then placed in a vibratome (VT1200S, Leica) for slicing, orthogonal to the pia to preserve cortical layers and white matter in proper orientation. Acute brain slices (300 μm in thickness) were made and maintained at 36 °C for ≥ 1 h in the recovery solution containing (in mM): 90 NaCl, 20 HEPES, 25 $NaHCO_3$, 2.5 KCl, 1.25 NaH_2PO_4, 20 D-glucose, 5 sodium ascorbate, 3 sodium pyruvate, 1 $CaCl_2$, 4 $MgCl_2$, pH adjusted to 7.3 with NaOH, 300-310 mOsm. All solutions were continuously aerated with carbogen (95% O_2, 5% CO_2) throughout the course of experiments, including transport and slicing, and refreshed every 6-8 hours. Experiments were performed within a period of typically 24 or 48 hours following resection, with exception (see Table 1). For rodent brain slices, 12-to-13-week-old male and female rats (Charles River) were anesthetized with isoflurane prior to decapitation; the cutting solution contained (in mM): 225 sucrose, 25 $NaHCO_3$, 2.5 KCl, 1.25 NaH_2PO_4, 20 D-glucose, 0.5 $CaCl_2$, 7 $MgCl_2$, 300-310 mOsm, and slices were recovered in artificial cerebrospinal fluid (aCSF) identical to the recording solution. A subset of the slices prepared for the current study was donated to be used elsewhere (Vardalaki et al., 2023). All protocols were approved by the internal review board (IRB) or the institutional animal care and use committee (IACUC) of the respective institution.

Whole-cell patch clamp

All human and rodent brain slice experiments were conducted under identical conditions. Slices were placed in a recording chamber and visualized with Dodt gradient contrast microscopy (Examiner Z1, Zeiss), while being perfused with the recording aCSF at 1.6 mL/min using a peristaltic pump (Minipuls 3, Gilson). The recording solution contained (in mM): 125 NaCl, 25 $NaHCO_3$, 3 KCl, 1.25 NaH_2PO_4, 10 D-glucose, 1.2 $CaCl_2$, 1.2 $MgCl_2$, 300-310 mOsm, maintained at 36 °C with an inline heating system (TC344C & SH28, Warner). Whole-cell patch clamp recordings were made from the soma of pyramidal neurons (PN) in layer 2/3 (L2/3) of the human neocortex, or L2/3 and L5 of the rat temporal association area (TeA), using a MultiClamp 700B amplifier (Molecular Devices). Data were bessel filtered at the cutoff frequency of 10 kHz, acquired at a sampling rate of 20 kHz, digitized and recorded with Prairie View (Bruker), then analyzed with PVBS (https://github.com/flosfor/pvbs). Patch pipettes (2.5-4.0 MΩ) were pulled from borosilicate glass capillaries (PG52151-4, WPI) with a horizontal pipette puller (P-1000, Sutter),

144 and positioned using a set of micromanipulators (Junior, Luigs & Neumann). The internal solution
145 contained (in mM): 130 K-gluconate, 4 KCl, 4 NaCl, 10 HEPES, 15 phosphocreatine-di(tris), 4 Mg-
146 ATP, 0.3 Na_2-GTP, adjusted to pH 7.3 with KOH, leading to final $[K^+]$ of ~136-138 mM, and 300-310
147 mOsm. Additionally, 0.05 mM Alexa Fluor 594 and 0.1 mM Oregon Green BAPTA-1 (Thermo Fisher)
148 were added to the internal solution for structural and calcium imaging. Pipette capacitance (C_p)
149 was fully compensated, typically ~13.5-14.5 pF. Series resistance (R_s) was continuously monitored
150 throughout the course of recordings, and cells with Rs ≤ 20 MΩ and change of less than 15% were
151 accepted. To measure the intrinsic neuronal membrane properties, cells were held in current
152 clamp at 0 pA, and injected at the soma with square current steps (-250 to +1000 pA in 50 pA
153 steps, duration 500 or 1000 ms), with bridge fully balanced. Input resistance (R_{in}) was calculated
154 from the linear regression crossing the origin from all subthreshold membrane potential
155 responses to step current input; for hyperpolarizing pulses, transient-state membrane potential
156 responses were used to minimize the contribution of hyperpolarization-activated current (i_h) in
157 calculating of R_{in}. Sag ratio was defined as the difference between the transient-state and the
158 steady-state membrane potential responses to -250 pA somatic current injection divided by the
159 former, in alignment with the definition of R_{in}. Transient-state responses were calculated as the
160 peak of the response in either direction, whereas steady-state responses were calculated as the
161 mean from the later 20% of the step duration. Resting membrane potential (RMP) was calculated
162 as the mean of the membrane potential during the baseline period preceding the current steps,
163 typically 500 ms. For action potential (AP) waveform analysis, the first AP generated at rheobase
164 was used. AP threshold was defined as the membrane potential immediately preceding the point
165 at which the derivative of the membrane potential with respect to time (dV/dt) first exceeded 10
166 (V/s); for this purpose, data were further processed with a 4th order bessel filter at the cutoff
167 frequency of 4 kHz for noise reduction. AP amplitude was calculated as the difference between
168 the AP peak and AP threshold, and the time between the two points at half of this amplitude
169 respectively from the depolarizing and the repolarizing phase was taken as AP half-width. Liquid
170 junction potential was measured at ~11-12 mV, but was not corrected for in the values of
171 membrane potential reported in the current study.

172

173 *2-photon glutamate uncaging and calcium imaging*

174 All experiments were conducted at the 2-photon core facility (46-6178) at the McGovern Institute
175 for Brain Research (MIBR), MIT. 2-photon excitation fluorescence microscopy (2PEF) for
176 simultaneous structural imaging, glutamate uncaging (2PGU), and calcium imaging was
177 performed using two Ti:sapphire lasers (Mai Tai eHPDS, Spectra Physics), modulated and guided
178 using a custom-built optical setup including electro-optic modulators (M350-80, Conoptics) and
179 an 8x pulse splitter (https://flosfor.github.io/pulse_splitter.pdf). Optical elements in the excitation
180 and emission pathways were obtained from Thorlabs, or Chroma in the case of optical filters,
181 unless otherwise specified. Signals were acquired with two photomultiplier tubes (H7422-40,
182 Hamamatsu), after wavelength separation. For structural and calcium imaging, cells were
183 visualized with Alexa Fluor 594 and Oregon Green BAPTA-1 as described above, respectively with
184 880 nm or 920 nm 2-photon excitation. For calcium imaging, line scans (256 repetitions of ~10
185 µm lines, each with ~1 ms duration at 8.25 µs/pixel) were made across the dendritic branch, near

186 the center of the synaptic spine cluster activated with 2PGU. The region of interest (ROI) and the
187 background for the fractional change in fluorescence (dF/F) were defined respectively as those
188 points with signal intensities above the 2nd percentile or below the 50th percentile from structural
189 imaging, with the ROI consisting of continuous points flanked by two segments each including
190 part of the background, during the baseline period prior to 2PGU pulse delivery. For 2PGU, 5 mM
191 MNI-caged-L-glutamate (Tocris) was dissolved in the recording aCSF (adjusted to 120 mM NaCl
192 from 125 mM to compensate for osmolarity), and delivered with minimal pressure using a puffer
193 pipette of pore diameter ~15-20 μm, positioned ~100 μm away from the synaptic spines. 2PGU
194 was achieved with 720 nm 2-photon excitation, quasi-simultaneously at an interval of 0.12 ms
195 between spines with a dual galvanometer scanner (Bruker), ~0.1 μm from the head of each
196 dendritic spine, at an intensity producing somatic uEPSPs within a range of physiological kinetics
197 and amplitudes, typically ~0.1-0.5 mV (typically between ~50-150 mW past the 63x objective
198 (421480-9900-000, Zeiss) in terms of the optical power of the excitation laser, but measured with
199 continuous full-field illumination instead of short, focalized pulses used for actual 2PGU
200 experiments). A total of 20-35 spines, typically spanning ~30-40 μm along a continuous segment,
201 were activated at a given dendritic branch.

202

203 *Data analysis*

204 Electrophysiology and calcium imaging data were analyzed and visualized using PVBS
205 (https://github.com/flosfor/pvbs). Structural imaging data were processed using imageJ
206 (https://imagej.net) with the MosaicJ plugin (http://bigwww.epfl.ch/thevenaz/mosaicj). Plots
207 were made using custom codes written in MATLAB (Mathworks), and Prism (GraphPad). Statistical
208 information was expressed as mean ± standard error of the mean (SEM), where n indicates the
209 number of branches or cells, as applicable. The skewness and the excess kurtosis of distributions
210 were denoted respectively by G_1 and κ; G_1 is the Fisher-Pearson standardized third moment
211 coefficient, and $κ = μ_4/σ^4 - 3$, where $μ_4$ is the fourth central moment and σ is the standard
212 deviation. Statistical comparisons were made with the Mann-Whitney U test, unless otherwise
213 specified. Spearman's rank correlation coefficient (ρ) was used to evaluate correlations. Linear
214 regressions were calculated based on the least squares method, whose slopes (m) were
215 compared using the F-test including their deviation from zero. Statistical significance was
216 accepted when the associated P value was below 0.05 ($*$ $P < 0.05$; $**$ $P < 0.01$; $***$ $P < 0.001$).

217

218

219 **Acknowledgements**

223

224